



Stimulated Raman scattering in 10 and 100 atmosphere molecular hydrogen
by Michael Jack Runkel

A thesis submitted in partial fulfillment of the requirements for the degree of Master of Science in
Physics

Montana State University

© Copyright by Michael Jack Runkel (1989)

Abstract:

This thesis presents a study of Stimulated Raman Scattering in 10 and 100 atmosphere molecular hydrogen using a broadband, multimode, xenon chloride excimer laser operating at ultraviolet wavelengths. Stimulated Raman Scattering was initiated in the medium using optimally aligned pump (308 nm) and Stokes (351 nm) beams. Raman gain data was collected for the cases of well-correlated and uncorrelated pump and Stokes beams. Theory was fit to data via numerical calculation using the multimode, fixed random phase and temporal square pulse models with variable pulse length as fitting parameter. Results of the data fits were compared to the results of previous work, used to compare the 10 and 100 atmosphere cases, and to account for differences between the correlated and uncorrelated results at fixed pressure. Comparison of the pulse times derived from numerical data fitting and from measurements of peak power density showed agreement to within the error bars found in the experiment.

Additional topics intended to supplement the main body of the thesis include a formal development of Riemann's method for the solution of second order hyperbolic partial differential equations, and its application to the Raman equations, and a characterization of molecular hydrogen as a Raman scattering medium using elementary quantum mechanics and spectroscopic theory.

**STIMULATED RAMAN SCATTERING IN 10 AND 100
ATMOSPHERE MOLECULAR HYDROGEN**

by

Michael Jack Runkel

**A thesis submitted in partial fulfillment
of the requirements for the degree**

of

Master of Science

in

Physics

**MONTANA STATE UNIVERSITY
Bozeman, Montana**

December 1989

N378
R867

APPROVAL

of a thesis submitted by

Michael Jack Runkel

This thesis has been read by each member of the thesis committee and has been found to be satisfactory regarding content, English usage, format, citations, bibliographic style, and consistency, and is ready for submission to the College of Graduate Studies.

11-27-89
Date

John L. Collins
Chairperson, Graduate Committee

Approved for the Major Department

11-27-89
Date

Robert J. Swenson
Head, Major Department

Approved for the College of Graduate Studies

12/18/89
Date

Henry L. Parsons
Graduate Dean

STATEMENT OF PERMISSION TO USE

In presenting this thesis in partial fulfillment of the requirements for a master's degree at Montana State University, I agree that the Library shall make it available to borrowers under rules of the Library. Brief quotations from this thesis are allowable without special permission, provided that accurate acknowledgment of source is made.

Permission for extensive quotation from or reproduction of this thesis may be granted by my major professor, or in his absence, by the Dean of Libraries when, in the opinion of either, the proposed use of the material is for scholarly purposes. Any copying or use of the material in this thesis for financial gain shall not be allowed without my written permission.

Signature Michael Runkel

Date November 27, 1989

ACKNOWLEDGEMENTS

I would like to thank my advisor, John Carlsten, for the opportunity to work on this project. He allowed me the freedom to pursue ideas on my own and consequently to take this project in any reasonable direction. As a result I have gained an education and experience of scope and depth which would not have been possible otherwise. The other members of this research group have also provided invaluable assistance. David MacPherson and Rand Swanson gave help on many sticking points during this work. Their assistance has been invaluable. Thanks are also due to Scott Remington for his help in collecting experimental data, which saved me a number of miles in running around the optical table, and for his expertise in computing. I am indebted to Phil Battle for frank and honest questions and concerns during the course of the numerical work and data fitting, and for pointing out many things that I had missed.

It is a rare opportunity for any student to have interacted with a teacher as eloquent as Dr. R. T. Robiscoe. I would like to express my gratitude for his lectures on mathematical physics, including hyperbolic partial differential equations, and Bessel functions which served me well in my research on Riemann's method and the solution of the Raman equations.

Thanks also to my other committee members, J. E. Drumheller, and G. Tuthill, for the time they took in reading my thesis and the revisions they suggested.

I would also like to express my appreciation to the secretaries of the Physics Department. Their help has been a great aid to the successful completion of this thesis.

I would never have brought this thesis to a successful conclusion if not for my wife Terry. She provided me with invaluable support and kept a level head when I had lost mine, and always saw to it that I did the right thing.

Finally, I would like to thank my parents for allowing me the freedom to pursue my goals, and for their continual interest in and support of my progress throughout my academic career.

TABLE OF CONTENTS

	Page
APPROVAL.....	ii
STATEMENT OF PERMISSION TO USE.....	iii
ACKNOWLEDGMENTS.....	iv
TABLE OF CONTENTS.....	v
LIST OF TABLES.....	vii
LIST OF FIGURES.....	viii
ABSTRACT.....	x
1. INTRODUCTION.....	1
2. ANALYTIC SOLUTIONS OF THE RAMAN EQUATIONS.....	6
Introduction.....	6
Theory.....	6
3. APPARATUS.....	13
Introduction.....	13
Data Acquisition and Reduction.....	16
4. LINEWIDTH MEASUREMENTS.....	19
Introduction.....	19
The Fabry-Perot Interferometer.....	19
Plate Separation Method.....	26
5. NUMERICAL ANALYSIS.....	29
Introduction.....	29
Modeling the Broadband Laser.....	30
The Riemann Integral.....	34
Program Testing.....	37
Data Fitting.....	40

TABLE OF CONTENTS - Continued

	Page
6. ANALYSIS, INTERPRETATION, AND CONCLUSION.....	45
Introduction.....	45
Experimental Data Characterization.....	46
Comparison to Previous Work.....	47
Comparison of 10 and 100 Atmosphere Results.....	48
Comparison of Correlated and Uncorrelated Results.....	49
Comments on the Temporal Square Pulse Model.....	50
REFERENCES CITED.....	52
APPENDICES.....	56
Appendix A - Riemann's Method.....	57
Appendix B - Computer Programs.....	63
GLATT.....	64
LFELD.....	66
RAMAN.....	71
AVEFIL.....	75
DEVIATION.....	78
Appendix C - Characterization of Molecular Hydrogen as a Raman Scattering Medium.....	81
Vibrational Spectra.....	83
Rotational Spectra.....	86
Summary.....	90

LIST OF TABLES

Table	Page
1. Pulse times derived from numerical fits to data.....	46

LIST OF FIGURES

Figure	Page
1. Three level energy diagram representing the Raman scattering process.....	7
2. Contour used in the solution of the Raman equations via Riemann's method.....	11
3. Schematic of experimental apparatus.....	14
4. Typical optical delay data showing the effect of smoothing.....	17
5. Theoretical output of an idealized Fabry-Perot.....	20
6. Typical digitized output of the Fabry-Perot operating in Fizeau mode.....	24
7. Schematic of apparatus used in measurement of the plate spacing.....	25
8. Fabry-Perot rotation angle as a function of order number.....	28
9. Typical electric field produced by the program LFELD.....	32
10. Typical temporal profile of the XeCl laser output.....	33
11. Numerical gain curve showing transient behavior.....	38
12. Numerical gain curves fit to 100 atm uncorrelated data.....	41
13. Numerical gain curve fit to 10 atm uncorrelated data.....	42
14. Numerical gain curves fit to 100 atm correlated data.....	43
15. Numerical gain curve fit to 10 atm correlated data.....	44
16. Contour used in developing generalized Riemann solution of hyperbolic partial differential equations.....	59
17. Contour used to adapt generalized Riemann solution to the Raman equations.....	62

LIST OF FIGURES - Continued

Figure	Page
18. Computer program GLATT	64
19. Computer program LFELD	66
20. Computer program RAMAN	71
21. Computer program AVEFIL	75
22. Computer program DEVIATION	78
23. Geometry used in determining the polarizability $\alpha_{z'z'}$ for Rotational Raman Scattering	88

ABSTRACT

This thesis presents a study of Stimulated Raman Scattering in 10 and 100 atmosphere molecular hydrogen using a broadband, multimode, xenon chloride excimer laser operating at ultraviolet wavelengths. Stimulated Raman Scattering was initiated in the medium using optimally aligned pump (308 nm) and Stokes (351 nm) beams. Raman gain data was collected for the cases of well-correlated and uncorrelated pump and Stokes beams. Theory was fit to data via numerical calculation using the multimode, fixed random phase and temporal square pulse models with variable pulse length as fitting parameter. Results of the data fits were compared to the results of previous work, used to compare the 10 and 100 atmosphere cases, and to account for differences between the correlated and uncorrelated results at fixed pressure. Comparison of the pulse times derived from numerical data fitting and from measurements of peak power density showed agreement to within the error bars found in the experiment.

Additional topics intended to supplement the main body of the thesis include a formal development of Riemann's method for the solution of second order hyperbolic partial differential equations, and its application to the Raman equations, and a characterization of molecular hydrogen as a Raman scattering medium using elementary quantum mechanics and spectroscopic theory.

CHAPTER ONE

INTRODUCTION

Raman scattering is a process whereby light, typically from a laser, interacts with a scattering medium, causing a frequency shifted photon to be emitted. As such, it is a three level process. The incident, or pump, photon drives the atom into a superposition of electronic states. The transition from the superposition state to a third state (a vibrational or rotational state of the lower electronic state) causes a photon, frequency shifted from the incident light, to be emitted. For a frequency downshift, the emission is known as Stokes radiation. Conversely, if the emission is higher in frequency it is known as Anti-stokes emission. Raman scattering was first observed by C. V. Raman¹⁹ in 1928.

Raman scattering can be viewed in at least two ways. The first treats the process in terms of small ensembles of atoms from the viewpoint of scattering theory²⁰, complete with derivatons of appropriate cross sections²¹. The second viewpoint concentrates on the derivation and solution of the "equations of motion" for the pump and Stokes electric fields propagating through large (macroscopic) mediums, and the coherence Q of the medium (i.e. the response of the medium to excitation). Of interest in this picture are the growth of the Stokes field (i.e. the gain), the depletion of the pump field, and the response of the medium to the fields. Numerous approaches have been used to obtain the equations of motion for the process. Historically, the equations have been derived semi-classically using Maxwell's wave equations for the fields with the nonlinear (induced) polarization of the medium acting as the driving term. It, in turn, is calculated from molecular susceptibilities. Earlier works^{1,2,22,23,24} used the Placzek model²⁵ of molecular

polarizability to obtain this term while later models^{3,26} used the quantum mechanical susceptibility. Shen and Bloembergen²², and Wang¹ derive the Raman equations using Lagrangian densities and Euler's equations. Raymer, Mostowski, and Carlsten³ employ the Bloch vector formalism and quantum mechanical susceptibilities in deriving the equations, while Raymer and Mostowski⁴ use a complete quantum (operator) description for the medium and Stokes fields, but treat the pump classically. Typically the Slowly Varying Envelope Approximation²⁷ and the Rotating Wave Approximation²⁷ are relied upon in all methods of derivation of the Raman equations.

The solution of the Raman equations was first presented in full form by Wang¹ using Riemann's method.^{13,14,15} Later, Raymer and Mostowski⁴ applied Laplace transform methods to obtain the solutions.

The pump sources used in Raman scattering fall into two categories: monochromatic (or nearly so) and broadband. Analysis of the Stokes field solution for monochromatic sources³ is rather straightforward and serves as a benchmark to which all other models are compared. For the broadband case, there exist numerous models to describe the scattering process. Among these is one known as the "multimode fixed random phase" model^{5,26,28}. In this model, it is assumed that an ensemble of atoms emits into a distribution of frequency modes which have constant amplitude and are weighted by a Lorentzian frequency distribution, which is caused by laser linewidth broadening mechanisms. Associated with the individual electric field of each mode is a random phase angle ϕ_n which accounts for the randomness of emission process of the excimer laser. The pump field is then taken to be the sum of a large number of the individual electric fields. The describing equation is $E = \sum_{n=-\infty}^{\infty} A_n \exp[-i(n\delta t + \phi_n)]$. Here δ represents the mode spacing of the laser.

When the pump intensity is very low, only spontaneous Raman scattering takes place. Initiation of the scattering process is due to quantum noise fluctuations³¹. If the

pump intensity is large enough, then the scattering process becomes stimulated or driven by the pump fields. For this case, Raman scattering can be divided into two categories. The first is Raman generation in which only the pump beam enters the medium and causes excitation. The second is Raman amplification in which both a pump beam and a Stokes probe are incident on the medium.

Theory²⁸ predicts that for generation, the Stokes intensity is independent of the number of modes, and that the pump and Stokes fields are highly (but not necessarily totally) correlated in phase. For amplification, however, the pump and Stokes fields become correlated in phase only at high gain values³, i.e., high input pump fields or long cell length. A further result is that the broadband gain falls below the monochromatic value at low pump energies or for short cells. Experimentally, the phase correlation issue has been explored by a number of authors^{29,30} who have verified the theoretical predictions.

This thesis is the continuation of research begun by Rifkin^{5,26}. It attempts to answer questions left behind from that work. Rifkin compared the predictions of the multimode fixed random phase model to experimental data for Raman scattering in molecular hydrogen at 100 and 10 atmospheres pressure. His results at 100 atm pressure matched the data quite well; however, fitting the data at 10 atm was not successful. Two factors attributed to the lack of fit at 10 atm include changing overlap in the pump and Stokes seed alignment in the experimental apparatus, and fluctuations in the laser linewidth between the times when 100 and 10 atm data were taken.

It is the goal of this thesis to investigate stimulated Raman scattering in 10 atm hydrogen and address the questions unanswered by Rifkin. This thesis will describe how the optical alignment was improved to give more stable measurements, as well as how the laser linewidth was monitored using a Fabry-Perot interferometer, which was unavailable at the time of Rifkin's work. Also described will be the numerical techniques used

to fit the data to the one parameter temporal square pulse model. As program testing and numerical calculations progressed, it became apparent that copious amounts of computing power would be necessary to properly address the issue of data fitting. At the time of Rifkin's work, such computing power was not readily available to him, making a protracted numerical analysis untractable, or impractical at best. To conclude the thesis a chapter will be given summarizing and interpreting the results of this project.

This thesis was assembled with the intent that the reader could gain the most important information with the first reading. Topics of secondary importance have been put into appendices for more detailed study later.

Chapter 2 presents the solution of the coupled Raman equations using Riemann's method. It is largely mathematical in content and omission of this chapter in first reading would not interrupt the continuity of the thesis. The most important results of this chapter are equations (2.1) and (2.25); the coupled differential Raman equations, and the integral solution for the Stokes field respectively.

Chapter 3 describes the experimental set-up, data collection and reduction techniques, and deals with experimental error bars as well.

Chapter 4 deals mainly with the role of the Fabry-Perot interferometer in this work. It discusses the basic concepts and jargon of Fabry-Perot interferometry and details how the instrument was used to monitor the lasers linewidth in real time. Included in this chapter is a description of a highly accurate optical method for determination of the Fabry-Perot plate spacing.

Chapter 5 is the core of this thesis. In this chapter is a discussion on the numerical methods used to generate the broadband laser field, and to evaluate the Stokes field solution derived in Chapter 2. The mathematical background is provided as well as a brief description of the computer codes involved. Further, Chapter 5 discusses the methods by which the computer codes were applied to fit the experimental data.

Chapter 6 discusses the results of this work. Here, the numerical results will be used to account for the features of the experimental data. The data fits will be given in terms of scaling arguments and pulse lengths derived from the numerical model found in Chapter 5. The results will also be compared to previous work, and concluding remarks regarding the one parameter temporal square pulse model in stimulated Raman scattering will be made.

Appendix A develops Riemann's method for solving linear second order hyperbolic partial differential equations. Riemann's method is a powerful, although somewhat delicate, tool which seems to have been lost to obscurity, likely superseded by more robust methods such as Laplace transformations.

Appendix B contains the Fortran source codes used in data analysis and numeric fitting.

Appendix C characterizes molecular hydrogen as a Raman scattering medium. Elementary spectroscopic models are called upon to determine the types of allowable Raman scattering (i.e. electronic, vibrational, or rotational Raman scattering), and it is shown that the Raman scattering seen in this experiment is mainly vibrational in nature.

CHAPTER TWO

ANALYTIC SOLUTIONS OF THE RAMAN EQUATIONS

Introduction

In this chapter the analytic solution to the transient Raman equations is derived using Riemann's Method (see Appendix A). The solution is presented in this thesis for a number of reasons. First, the emphasis in the literature appears to be in the derivation of the Raman equations, with the solution merely being quoted. Secondly, the solutions for E_s and Q^* presented by Wang¹ are in notation which is non-transparent. For these reasons, it seems appropriate to include the full derivation of the integral solution for the Stokes field $E_s(z, \tau)$. It should be noted that Riemann's Method is not the only way to solve the Raman equations. They are susceptible to solution using Laplace transforms as well⁴. The solution readily lends itself to numeric evaluation as will be discussed in Chapter 5.

Theory

In solving the Raman equations, the procedure of Carman et. al.² will be followed, but the equations shall be written in a more standard notation. The Raman equations are³

$$\frac{\partial Q^*}{\partial t} + \Gamma Q^* = i\kappa_1 E_s E_L^* \quad (2.1a)$$

and

$$\frac{\partial E_s}{\partial z} = -i\kappa_2 Q^* E_L \quad (2.1b)$$

Q^* denotes the coherence of the medium, Γ is the Raman linewidth of the medium, E_s and E_L refer to the Stokes and pump (laser) fields respectively, and κ_1 and κ_2 are the coupling constants having the form given by Raymer et. al.³ of

$$\kappa_1 = \frac{d_{12}d_{23}}{2\hbar^2\Delta_L} \quad (2.2a)$$

and

$$\kappa_2 = \frac{\pi N \omega_s v_s d_{12}d_{23}}{c^2 \hbar \Delta_L} \quad (2.2b)$$

Here d_{ij} refers to the dipole matrix element between states i and j , v_s is the velocity of propagation in the medium, and Δ_L is the detuning from the $|1\rangle \rightarrow |2\rangle$ transition.

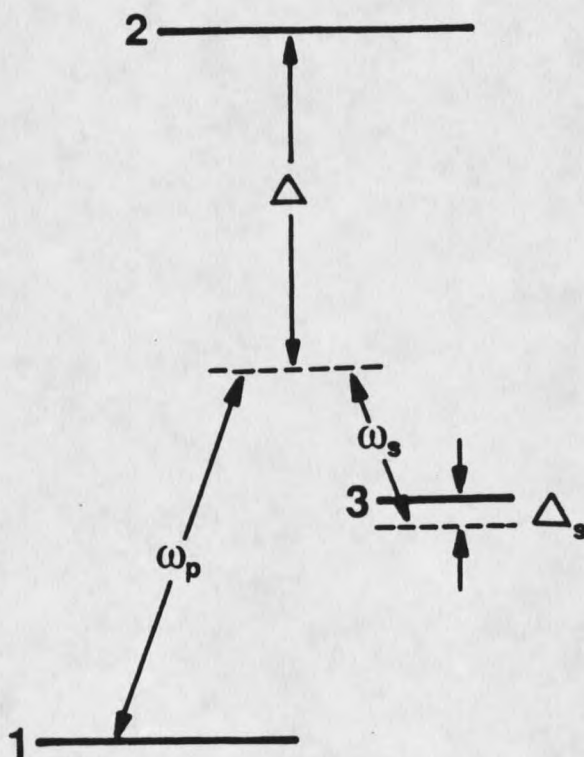


Figure 1. Three level energy diagram representing the Raman scattering process. ω_p and ω_s denote the pump and Stokes frequencies and Δ_L and Δ_s the detunings from resonance. $|1\rangle$ and $|2\rangle$ are electronic levels, while $|3\rangle$ denotes a vibrational level of the state $|1\rangle$ which is typically the electronic ground state.

The variables t and z refer to a reference frame which is comoving with the pulse. They are connected to the laboratory frame by the relations $t = t' - z/v_s$ and $z = z' - v_{pho}t$ and it is assumed that $v_{pho} \ll c$ where v_{pho} refers to the phonon velocity in the medium. Also, the assumption is made that the group velocities of the pump and Stokes are matched and that no pump depletion or medium saturation occurs during the scattering process. Consequently, the laser field may be written as $E_L = E_L(t)$. The Raman equations (2.1) may be decoupled in the classical manner as follows. Rewrite (2.1b) as

$$Q^* = \frac{i}{\kappa_2 E_L} \frac{\partial E_S}{\partial z} \quad (2.3)$$

and take its time derivative to get

$$\frac{\partial Q^*}{\partial t} = \frac{i}{\kappa_2} \left(-\frac{1}{E_L^2} \frac{\partial E_L}{\partial t} \right) \frac{\partial E_L}{\partial z} + \frac{i}{\kappa_2 E_L} \frac{\partial^2 E_S}{\partial z \partial t} \quad (2.4)$$

Substitution of (2.3) and (2.4) into (2.1b) eliminates all Q^* dependence. The result is

$$\left(-\frac{1}{E_L^2} \frac{\partial E_L}{\partial t} \frac{\partial E_S}{\partial z} + \frac{1}{E_L} \frac{\partial^2 E_S}{\partial t \partial z} \right) + \Gamma \frac{\partial E_S}{E_L \partial z} = \kappa_1 \kappa_2 |E_L|^2 E_S \quad (2.5)$$

Using $E_L = E_L(t)$ equation (2.5) can be written as

$$\frac{\partial^2}{\partial z \partial t} \left(\frac{E_S}{E_L} \right) + \Gamma \frac{\partial}{\partial z} \left(\frac{E_S}{E_L} \right) - \kappa_1 \kappa_2 |E_L|^2 \left(\frac{E_S}{E_L} \right) = 0 \quad (2.6)$$

If the same procedure is applied to (2.1) to eliminate the E_S dependence, the decoupled Q^* equation is

$$\frac{\partial^2 Q^*}{\partial z \partial t} + \Gamma \frac{\partial Q^*}{\partial z} - \kappa_1 \kappa_2 |E_L|^2 Q^* = 0 \quad (2.7)$$

Letting $F = Q^*$ or E_S/E_L equations (2.6) and (2.7) take the form

$$\frac{\partial^2 F}{\partial z \partial t} + \Gamma \frac{\partial F}{\partial z} - \kappa_1 \kappa_2 |E_L|^2 F = 0 \quad (2.8)$$

The first derivative in z can be eliminated through the transformation $F(z, t) = U(z, t)e^{-\Gamma t}$. Calculating derivatives shows that

$$\frac{\partial F}{\partial z} = U_z e^{-\Gamma t} \quad (2.9a)$$

and

$$\frac{\partial^2 F}{\partial z \partial t} = e^{-\Gamma t} (U_{zt} - \Gamma U_z) \quad (2.9b)$$

with the subscripts denoting partial derivatives. Substitution gives the equation

$$U_{zt} - \kappa_1 \kappa_2 |E_L(t)|^2 U = 0 \quad (2.10)$$

Equation (2.10) can be simplified further if the change of variables

$$p(t) = \int_{-\infty}^t |E_L(\xi)|^2 d\xi \quad (2.11)$$

is applied. It should be noted that p is proportional to the energy in the laser pulse up to the time t . Again, calculation of appropriate derivatives shows

$$U_t = U_p |E_L|^2 \quad (2.12a)$$

and

$$U_{tz} = U_{pz} |E_L|^2 \quad (2.12b)$$

Equation (2.10) becomes

$$\frac{\partial^2 U}{\partial p \partial z} - \kappa_1 \kappa_2 U = 0 \quad (2.13)$$

This is (2.8) transformed to normal form. The variables p and z are the normal coordinates. The initial conditions of interest given by Carmen et. al.² are

$$\partial E_s / \partial z = Q^*(z) = 0 \quad (2.14a)$$

at $t = -\infty$, and

$$E_s(t, 0) = E_0 \quad (2.14b)$$

The first equation above is the condition that there is no excitation in the medium before the laser pulse arrives. The second is just the input Stokes field at the entrance of the Raman cell. Translated into the notation of (2.13) they become

$$\frac{\partial U}{\partial z} = 0, \text{ and } U(p, 0) = U_0 \quad (2.15)$$

Riemann's Method can now be applied to (2.13). The first step is to find the Riemann function v for the problem. Since $a(p, z) = b(p, z) = f(p, z) = 0$ in (2.13), the associated Riemann function equation is

$$v_{pz} - \kappa v = 0 \quad (2.16)$$

Here, $\kappa = \kappa_1 \kappa_2$. To solve (2.16) let $v(p, z; \alpha, \beta) = F(s)$ where $s = (p - \alpha)(z - \beta)$. This transformation will change (2.16) into an ordinary differential equation. Repeated application of the chain rule allows (2.16) to be written as

$$sF_{ss} + F_s - \kappa F = 0 \quad (2.17)$$

Define a new variable λ via $\lambda = \sqrt{4\kappa s}$ and transform, again using the chain rule repeatedly, to obtain the Modified Bessel equation of order zero

$$F_{\lambda\lambda} + \frac{1}{\lambda} F_{\lambda} - F = 0 \quad (2.18)$$

The solution to (2.18) is

$$v(p, z; \alpha, \beta) = I_0[\sqrt{4\kappa(p - \alpha)(z - \beta)}] \quad (2.19)$$

Explicit calculation shows that v fulfills the conditions (given in equation (A.9) of Appendix A) placed on Riemann-Green functions.

To complete the solution it remains to evaluate equation (A.15) of Appendix A. In p and z notation it reads

$$u \Big|_{P=(p,z)} - uv \Big|_{R=(p,0)} = - \int_0^p u \frac{\partial v}{\partial p'} dp' + \int_0^z v \frac{\partial u}{\partial z'} dz' \quad (2.20)$$

The integration contour is shown in Figure 2.

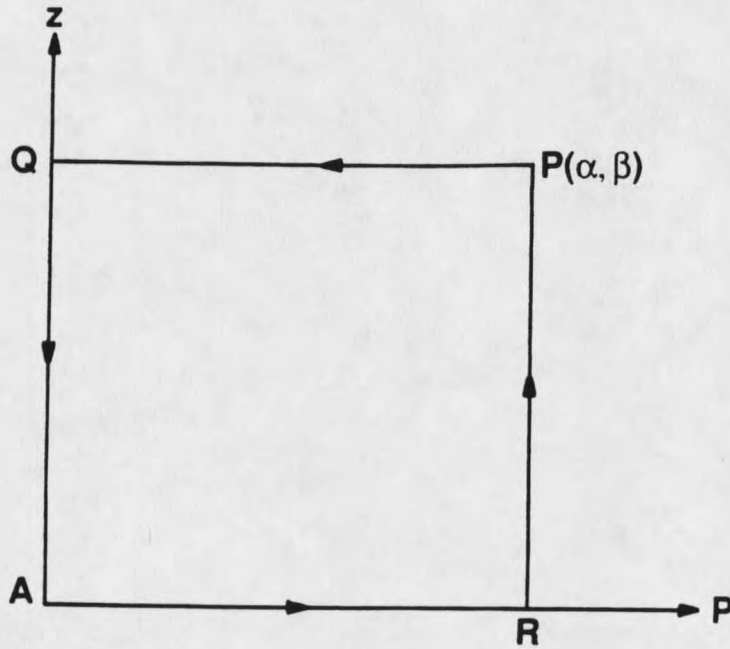


Figure 2. Contour used in the solution of the Raman equations via Riemann's method. The boundary conditions are stipulated along the p and z axes.

The second integral vanishes due to the initial condition (2.15). The first integral is evaluated as follows

$$\int_0^p uv_p dp' = \int_p^0 u(p', 0) \frac{\partial}{\partial p'} I_0 \sqrt{4\kappa z} (p - p') dp' \quad (2.21)$$

Here $\beta = 0$ as shown in Figure 2. Calculating the derivative of the Bessel function gives the result

$$\int_0^p u v_p dp' = - \int_0^p u(p', 0) \left(\frac{\kappa z}{p - p'} \right)^{1/2} I_1 \sqrt{4\kappa z (p - p')} dp' \quad (2.22)$$

Now, transform back to original variables using $dp = |E_L(t)|^2 dt$ and

$E_S(t)/E_L(t) = U \exp(-\Gamma t)$ and appropriate dummy indicies. The complete result is

$$E_S(z, t) = E_S(0, t) + \sqrt{\kappa_1 \kappa_2 z} E_L(t) \int_{-\infty}^t e^{-\Gamma(t-t')} E_L^*(t') E_S(0, t') \frac{I_1[\sqrt{4\kappa_1 \kappa_2 z (p(t) - p(t'))}]}{\sqrt{p(t) - p(t')}} dt' \quad (2.23)$$

By similar methods it can be shown that the coherence may be written as

$$Q^* = i\kappa_1 \int_{-\infty}^t e^{-\Gamma(t-t')} E_L^*(t') E_S(0, t') I_1[\sqrt{4\kappa_1 \kappa_2 z (p(t) - p(t'))}] dt' \quad (2.24)$$

To be consistent with notation used by Raymer et. al.³ let $t \rightarrow \tau$ and change limits from $-\infty$ and t to 0 and τ . For the dummy variable t' the Stokes field solution reads

$$E_S(z, \tau) = E_S(0, \tau) + \sqrt{\kappa_1 \kappa_2 z} E_L(\tau) \int_0^\tau \frac{E_L^*(\tau') E_S(0, \tau')}{\sqrt{p(\tau) - p(\tau')}} e^{-\Gamma(\tau-\tau')} I_1[\sqrt{4\kappa_1 \kappa_2 (p(\tau) - p(\tau'))}] d\tau' \quad (2.25)$$

CHAPTER THREE

APPARATUS

Introduction

It is the goal of this work to investigate the theory of stimulated Raman scattering with broadband lasers. In principle, the experiment should be designed and executed with the versatility to probe as many of the theoretical predictions as possible. In practice, however, this usually proves to be impractical for various reasons and the experiment may need to be restricted in scope. To that end, this experiment was designed to examine the Raman gain as a function of the correlation between temporal envelopes of the pump and Stokes beams, their respective energies and response to changes in the medium. This was achieved in the following manner.

The laser light used in this experiment was produced by an injection locked Lambda Physik EMG 150 ET pulsed, gas discharge excimer laser using xenon chloride as the lasing medium. This laser and its broadband characteristics are well described by Rifkin⁵ and will not be discussed in this thesis, save for a brief description given in Chapter 5. The laser was tuned to operate on the 308.15 nm spectral line of the XeCl, i.e. in the ultraviolet. The pulses produced had a characteristic temporal length of 13.5 ns and energy of 150 mJ typically. Hence, the average power output per pulse was on the order of ten Megawatts.

For use in the experiment, the beam was made diffraction limited by clipping it with

a circular aperture 4.5 mm in diameter, and reduced in energy as needed along the beam path through the use of appropriate dielectric attenuators.

As shown in Figure 3, the beam was divided into two parts by a beam splitter.

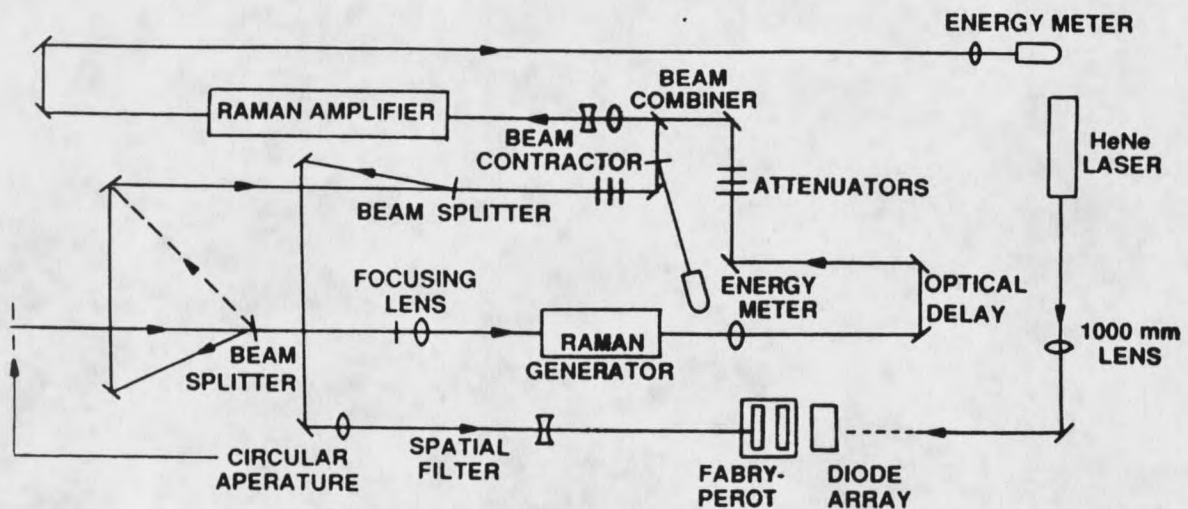


Figure 3. Schematic of experimental apparatus. The dashed line in the UV beam denotes the optical path before modification to improve beam alignment. The dashed HeNe beam indicates usage only for plate spacing measurements.

The transmitted portion was brought to focus at the center of the 50 cm Raman generator cell by a 1 m lens. Before entering this cell, the light was appropriately attenuated to prevent the generation of higher order Stokes processes. Upon exit from this cell, the frequency shifted Stokes light was collimated by another lens. A 100 cm lens was used at 100 atm pressure and a 75 cm lens at 10 atm. These lenses kept the spatial profiles of the Stokes beam comparable in the amplifier cell when the pressure in the cells was changed from one experiment to the next. Next, the Stokes beam passed through the optical delay. The delay consisted of a 3 mirror corner cube mounted on a linear motor drive. With this arrangement, it was possible to make changes of 80 mm (270 ps) in the

optical path length of the Stokes leg. As such, the delay acted as a correlation control device between the pump and Stokes beams. Theory^{3,28} predicts that the spontaneously generated Stokes light will become correlated with the pump beam for high gain, which occurs in the generator cell. Hence, if the pump and Stokes legs have the same optical path length, then the two beams should be highly correlated when they reach the amplifier. Once past the delay, the Stokes beam was suitably attenuated and brought to the beam combiner.

The remaining beam, known as the pump beam, travelled a path length comparable to that for the Stokes (within the range provided by the optical delay) and when attenuated as desired was placed directly on the Stokes beam at the beam combiner. The beams were then sent into a beam contracter composed of the 500 and -250 mm lens combination whereupon they passed into the 100 cm Raman amplifier cell. After passing through the amplifier the residual 308 nm wavelength was filtered out and the Stokes energy measured (as a function of delay).

The Raman medium of choice was molecular hydrogen (H_2) and was used in both the generator and amplifier. Molecular hydrogen is a well understood Raman scattering medium and is characterized in Appendix C. The experiment was done twice: initially at 100 atm pressure, and then at 10 atm pressure. These pressure changes served not only to change the Raman linewidth of the medium, but the value of the coupling constant κ_2 in the Raman equations (see Chapter 2). In essence, the experimental apparatus was the same as that used by Rifkin⁵ in prior work, however, modifications to the pump leg were made to improve the sensitivity. Initially, Rifkin's work at 100 atm was repeated for verification purposes, but when reduced, the gain enhancement data showed unacceptable scatter. While this was attributed to lack of familiarity with the experimental technique, it also prompted an investigation into making the experimental method more reliable. The problem was due to the so-called "pointing average"; the random movement of the

